

Prestack migration by equivalent offsets and CSP gathers: an update

John C. Bancroft, Hugh D. Geiger, Shaowu Wang, and Darren S. Foltinek

ABSTRACT

A method of prestack time migration is presented that is simpler, faster, and provides more information than conventional methods. The method is based on principles of prestack Kirchhoff time migration, and can be applied to both 2-D and 3-D data. Common scatter point (CSP) gathers are created in an intermediate step for each output migrated trace, similar to prestack imaging (PSI) gathers presented by Forel and Gardner (1988). Normal moveout (NMO) and stacking of CSP gathers is all that is required to complete the prestack migration process. This new method allows the CSP gathers to be formed at any arbitrary location for velocity analysis, or prestack migrate a 2-D line from a 3-D volume.

The CSP gather is similar to a CMP gather, as both contain offset traces, and both represent a vertical array of scatter points or reflectors. However, the CSP gather is superior with a greater number of traces, and a larger maximum offset. All the input traces within the migration aperture are used to form the CSP gather. Samples in the input traces are assigned an equivalent offset for each CSP location, then copied into the appropriate offset bin of the CSP gather in an efficient manner. The input time samples remain at the same time when copied to the CSP gather. Data in the CSP gathers may be scaled, filtered, or have noise attenuation processes applied.

The prestack nature, high fold, and large offsets aid in providing a better focus of the semblance plot for an improved velocity analysis. Another benefit of the process is its speed, which combines many prestack arithmetic computations. Additional computation time is saved when amplitude scaling and anti-aliasing filtering are performed on the bins of the CSP gathers.

INTRODUCTION

Migration is a process that attempts to reconstruct an image of the original reflecting structure from energy recorded at the surface in seismic traces. Early processing expended a great deal of effort to produce a stacked section from common mid point (CMP) gathers, followed by a post-stack migration based on the stacking velocities. Stacking velocities however, require higher velocities for dipping events (Gardner 1947 and Dix 1955) than those required for post stack migration, and some form of migration velocity estimation became a requirement. Further processing advances recognized that smearing from dip compensated velocities could be corrected by the inclusion of dip moveout (DMO) (Deregowski 1986) and prestack migration. The use of these prestack processes in velocity analysis loops enabled a more accurate estimate of the subsurface velocities and improved sub surface images.

DMO and post stack migration is currently more economical than conventional prestack migration, consequently the DMO method tends to be the current processing standard. However, the use of DMO should be restricted to areas with smoothly varying velocities. In areas where the smooth velocity criteria fails, prestack migration should be the preferred processing method. Typical prestack migration methods include migration of source (or shot) records (Schultz 1980, van der Schoot 1989, Lee 1992, Ng 1993), migration of constant (or limited) offset sections (Sattlegger 1980, Deregowski 1990), and migration by alternating downward continuation between shot gathers and geophone (S-G) gathers (Diet 1993, Denelle 1986). The Kirchhoff method may be a part of these (and other) migration algorithms. Full prestack Kirchhoff migration (Lumley et al. 1989, 1993) is a stand-alone process described by summation of input samples directly to the output migrated sample. It may appear that prestack migration methods are the most recent theoretical developments, however, the basics of some theoretical prestack migrations date back to developments in the early 1970's in papers by Lindsey (1970) and Rockwell (1971). The common use of full prestack migrations continues to be limited by computer hardware and long run times.

The method presented in this paper is based on the principles of prestack Kirchhoff migration. Rather than move input energy directly to the migrated position, an intermediate step is included to gather the energy before NMO.

The following section will evaluate the conventional processing procedures from the vantage point of prestack time migration. The Cheop's pyramid will be used to compare the different methods, and how they relate to prestack migration.

PRESTACK MIGRATION MODEL

The full Kirchhoff approach to prestack migration is based on a model of scatter points that will scatter (or reflect) energy from any source to any receiver. A reflecting event is composed of an organized arrangement of scatter points that produce a diffuse reflection. This is in contrast to the CMP assumption that assumes specular reflections from mirror like reflectors. The surface position of a vertical array (or trace) of scatter points is referred to as the *common scatter point* (CSP) location. The objective of prestack migration is to gather all the scattered energy and relocate it at the position of the scatter points. The traditional approach to Kirchhoff prestack migration begins by assuming an output location (or scatter point), and then gathers the appropriate energy from all available input traces. This procedure is repeated for every output sample.

The reflection time of scattered energy in each input trace, (relative to a scatter point), is identified by the travel time of the raypath between the source, scatter point, and receiver. Ray path travel times may be estimated by a number of different methods, such as ray tracing, or wave front computations, to produce a *depth* migration.

The travel time computation may be simplified to assume linear ray paths from the source to scatter point, and from the scatter point to receiver as illustrated in Figure 1. Travel times are computed using the geometry and a velocity that is defined for each scatter point. The migration velocity is usually equated to an RMS velocity. Results using this method are referred to as a *time migration*. After time migration the samples in a trace follow the time and path of an image ray. Use of image rays enable a conversion of the time migration to an estimate of the depth migration. Consequently, time migrations are used to aid in defining the velocity fields used in depth migration.

The contents of this paper are based on the time migration approach.

Kirchhoff prestack time migration

The total travel time T is estimated from the source to scatter point time T_s , and the scatter point to a receiver time T_r by

$$T = T_s + T_r. \quad (1)$$

The raypath times T_s and T_r are estimated with equations similar to the NMO equation, and the geometry of Figure 1. Conventional use of the NMO equation and other post stack processes use the two-way zero offset time T_0 to represent the zero offset travel time from a position immediately above the scatter point. However, for prestack computations, it is preferable to use the one-way, or half T_0 time $\frac{1}{2}T_0$, to simplify the prestack equations. The source and receiver distances h_s and h_r are measured from the CSP location, and the migration velocity V_{mig} is defined at $\frac{1}{2}T_0$, independent of h_s and h_r . Equation (1) then becomes the double square root (DSR) equation

$$T = \sqrt{\frac{1}{2}T_0^2 + \frac{h_s^2}{V_{mig}^2(T_0)}} + \sqrt{\frac{1}{2}T_0^2 + \frac{h_r^2}{V_{mig}^2(T_0)}}. \quad (2)$$

The prestack Kirchhoff migration algorithm typically works with one scatter point at a time, and searches all the input traces for energy that has been scattered. The travel time T is computed for each input trace within the migration aperture, the energy at that time is filtered, scaled and then summed into the migrated sample. The energy gathered into the migrated sample will constructively (or destructively) sum to recreate the structure of the subsurface. The filtering of the input traces is necessary to prevent aliasing noise (Silva 1992, Lumley 1993 and 1994) in the reconstructed image, and will vary for different scatter point locations. The amplitude weighting of the input samples also varies with each input trace. The anti-aliasing filter and amplitude weighting add significant computational overhead to the migration algorithm.

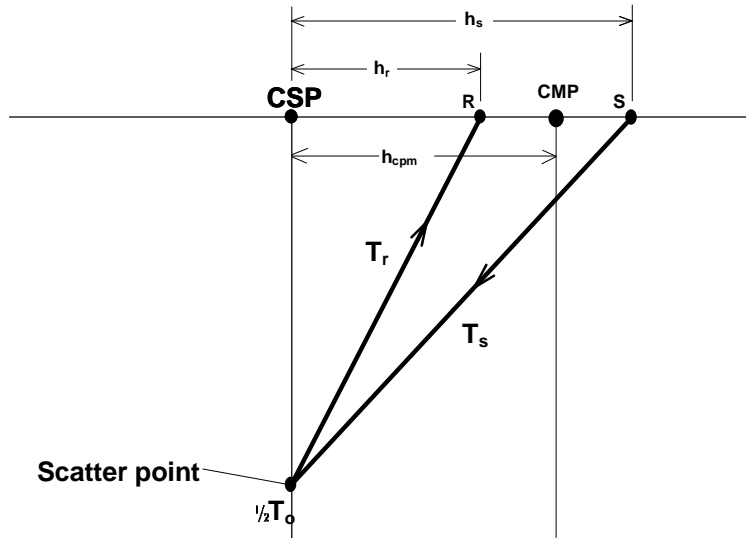


Figure 1 Geometry for prestack Kirchhoff time migration.

Cheop's pyramid

The two-way travel time T may be computed from one scatter point to a continuum of 2-D source and receiver locations, and displayed as a surface in a three dimensional volume. The axis of the volume are CMP location, source/receiver half offset h , and time t . This surface is known as Cheop's pyramid (Claerbout 1984 pages 164-163), and an example is shown in Figure 2a. For comparison purposes, an hyperboloid, which is hyperbolic in any vertical plane is shown in Figure 2b. The Cheop's pyramid has two hyperbolic planes that are identical to the hyperboloid; one at zero offset, and the other at the scatter point gather. All other points on Cheop's pyramid differ from the hyperboloid. This difference is observed by comparing the left edge of

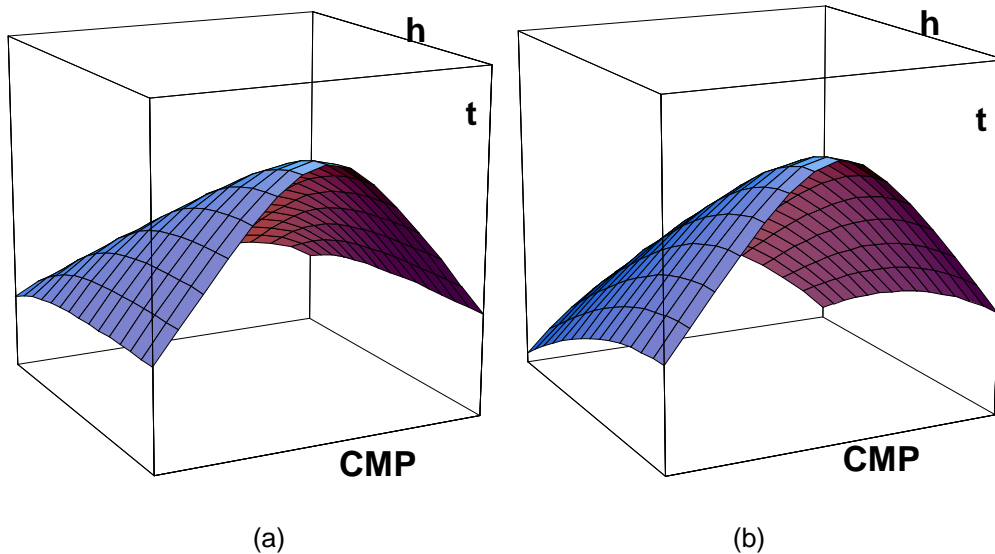


Figure 2. Perspective view of a) Cheop's pyramid, and b) a hyperbola created from the same scatter point (possibly by a Gardner DMO).

the surfaces in Figures 2a and 2b. The edge of Figure 2a shows that energy coming from an out-of-CMP-plane scatter point is distributed with non-hyperbolic moveout.

Conventional processing that is based on CMP gathers, is forced to ignore the non-hyperbolic distribution of energy, and limit the resolution in structured areas. In contrast, *true prestack migration methods are based on the non-hyperbolic energy distribution* defined in equation (2). The various processing schemes may now be evaluated on the basis of how well they collect energy on the Cheop's pyramid, and place it back at the scatter point, or apex of the pyramid.

In real data, the location of energy on the pyramid surface will be determined from the reflection strength of the neighbouring scatter points. Horizontal linear reflectors will tend to concentrate energy at the top portion of the pyramid, while dipping reflectors will tend to have more energy at the corresponding seismic dip. Energy from edges, such as faults, will be dispersed more evenly over the surface. The velocity of data on the pyramid is defined at the apex, or scatter point location, even though it may extend into areas with complex velocity structures. The above Cheop's pyramid was defined for 2-D data. Energy from a scatter point in 3-D data may also be mapped into a Cheop's pyramid by substituting other parameters for the CMP location and half source/receiver offset.

Scatter point energy with same T_{0-nmo}

The distribution of this energy in a CMP gather is illustrated in Figure 3, with three scatter points located with the same zero offset travel times T_{0-nmo} . This model uses a constant velocity model. Figure 3a shows raypaths to the three scatter points on a cross section with the deepest scatter point located at the CMP location. The other two scatter points are displaced to one side. The energy in the two sided CMP gather of Figure 3b will form where the Cheop's pyramid from each scatter point in Figure 3c intersects the CMP plane. The left side of Figure 3c also displays one side of the same CMP gather.

Figure 3 illustrates the problem with dispersed scatter point energy on a CMP gather. One of the scatter points is located at the CMP and has a hyperbolic shape while the other two scatter points lie off the CMP plane and produce a non-hyperbolic shape. NMO can only image correctly the one scatter point, even in a constant velocity environment. The hyperbolic moveout would represent energy from a horizontal reflector. The other scatter points with non-hyperbolic moveout represent dipping reflectors, and could be partially imaged by increasing the velocity used for NMO to match the curvature at zero offset with a hyperbola.

These figures reveal that in a constant velocity medium, NMO can not correctly image the sub-surface.

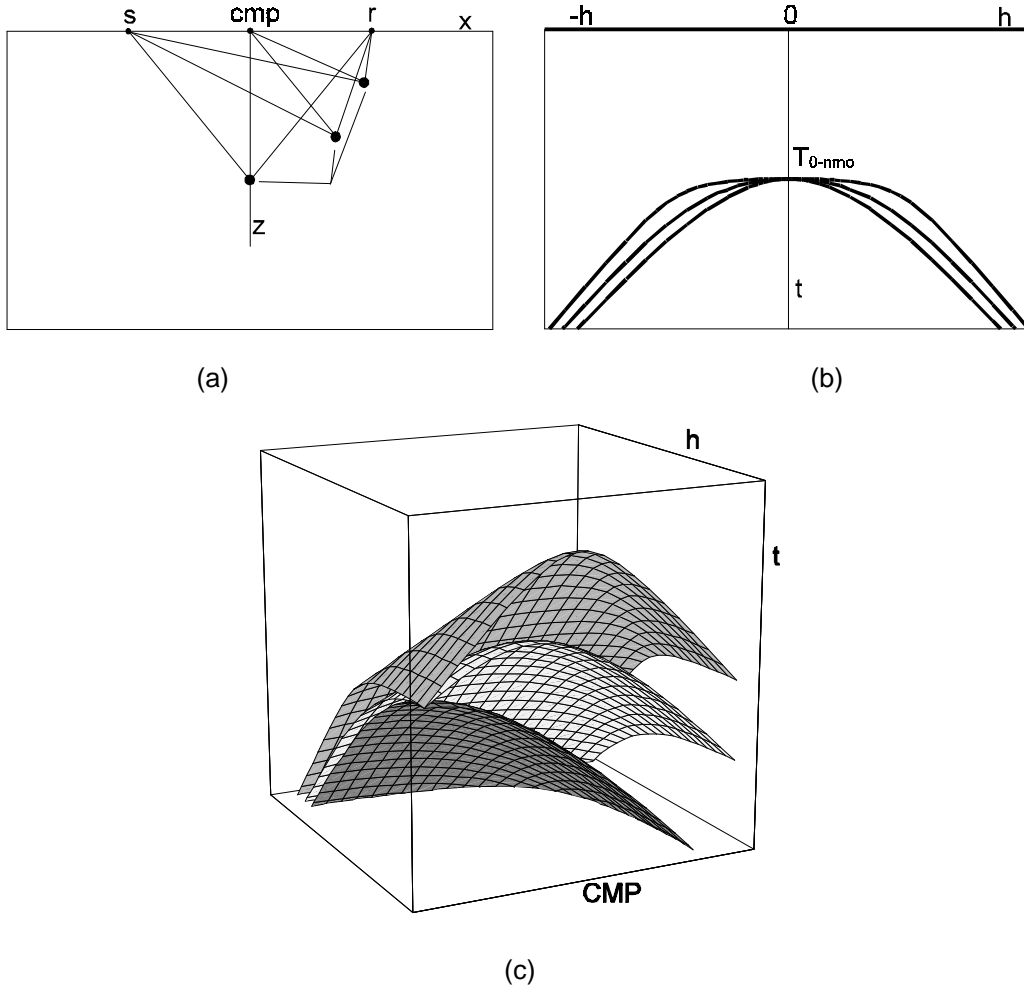


Figure 3. Three scatter points having the same zero offset T_0 at a given CMP with a) showing their position in a 2-D line, b) the CMP gather located at the same position as the lower scatter point, and c) the three Cheop's pyramid in a prestack volume.

COMPARISONS OF STANDARD PROCESSING TO PRESTACK MIGRATION

The performance of different processing methods may be evaluated by comparing how well they gather energy from the surface of Cheop's pyramid. The following section is intended to review and reveal the limitations of standard processing sequences. It is assumed that statics, amplitudes, deconvolutions, and velocity have been correctly identified and applied where appropriate.

NMO and stacking dipping events

Constant velocity medium

The preceding section showed three scatter points in Figure 3c in a constant velocity medium. Figure 4 illustrated the application of NMO to the same volume.

Only CMP gathers at the respective scatter points will have the correct moveout, implying only horizontal events can be corrected with NMO.

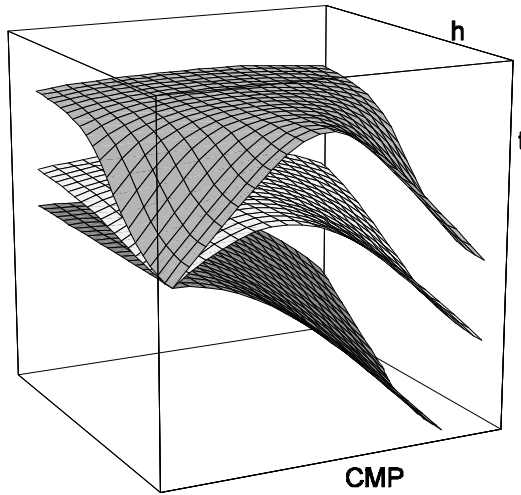


Fig. 4. Cheop's pyramid with the application of constant velocity NMO.

Variable velocity media

Dipping events are modelled from a series of scatter points and their energy will tend to align along the non-hyperbolic curves illustrated above. Semi-optimum stacks can be achieved by increasing the stacking velocity to achieve a best match of the non-hyperbolic curves with hyperbolas. The curvature of the Cheop's pyramid may be found from the second derivative of the DSR equation (2) and matched with the second derivative of the appropriate NMO hyperbola. Solving for the stacking velocity V_{stk} (Appendix 1) yields

$$V_{stk} = V \frac{T_{0-nmo}}{T_{0-mig}} = \frac{V}{\cos(dip)}, \tag{3}$$

which is the familiar velocity correction required for stacking a dipping event. Note the velocity V is the velocity at the scatter point T_{0-mig} and not at the NMO time T_{0-nmo} . Only the energy close to zero offset will be stacked using this method of processing.

Another interesting observation from equation (3) is the definition of a velocity function that will always produce a stack semi-optimized for dip. For a given scatter point, V/T_{0-mig} is constant c allowing equation (3) to become

$$V_{stk} = cT_{0-nmo}. \tag{4}$$

When the RMS type velocities are increasing proportional to time, regular NMO will produce a stack semi-optimized for all scatter points and all dips, as illustrated in Figure 5. DMO should not be used with this type of data where the RMS velocity increases proportionally with time.

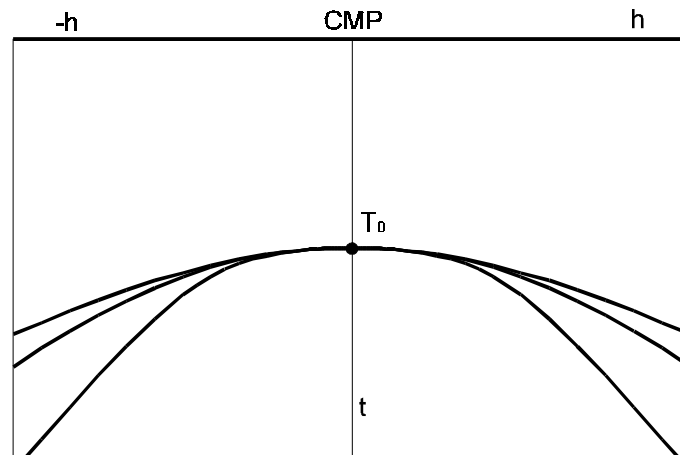


Figure 5. A CMP gather displaying energy from three scatter points. The velocity at each scatter point increases linearly with time.

The Cheop's pyramid also illustrates the use of infinite velocities to obtain a brute stack of steeply dipping events. Note in Figure 3c the Cheop's pyramid from the upper scatter point is tending to be flatter at zero offset. Steeper dips are represented farther down the pyramid where the zero offset tends to zero, and can produce a reasonable stack without NMO.

Conventional DMO

Constant velocity media

The inclusion of conventional DMO after NMO may convert the surface of Cheop's pyramid to one that maps the zero offset hyperbola across all offsets, producing the cylindrical hyperbola illustrated in Figure 6. The scattered energy is now at the correct time and ready for stacking. In a *constant velocity* environment, all the Cheop's pyramids would be converted to cylindrical hyperbolas that will align in any CMP gather. However, when the velocity varies, only one NMO velocity at T_{0-nmo} can be applied for all the scatter points to prevent energy from aligning within the CMP gather.

Variable velocity media

The application of DMO has been successful in areas where the velocity varies smoothly to approximate the constant velocity condition. In areas where the velocity varies caution must be used when using conventional DMO as it may degrade rather than help image the data. Special routines are available that allow DMO in complex velocity areas, and their use is balance with the use of prestack migration. Figure 7 shows two images NMO and NMO and DMO applied to data in which the velocity increases by

$$V(t) = V_0(1 + 0.5t). \quad (5)$$

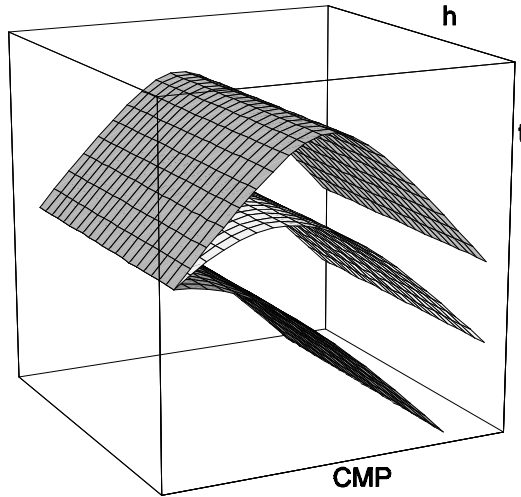


Fig. 6. NMO of data in Figure 4.

The scale in the figures range from 0 to 2.0 seconds, 0 to 2000 m in the CMP direction, and a maximum offset of 2000 m. The velocity at t_0 is 2000 m/s. Note the CMP gathers on the left side of each figure. Neither CMP gather aligns the data, and a preferred choice is not clear for the given velocity function.

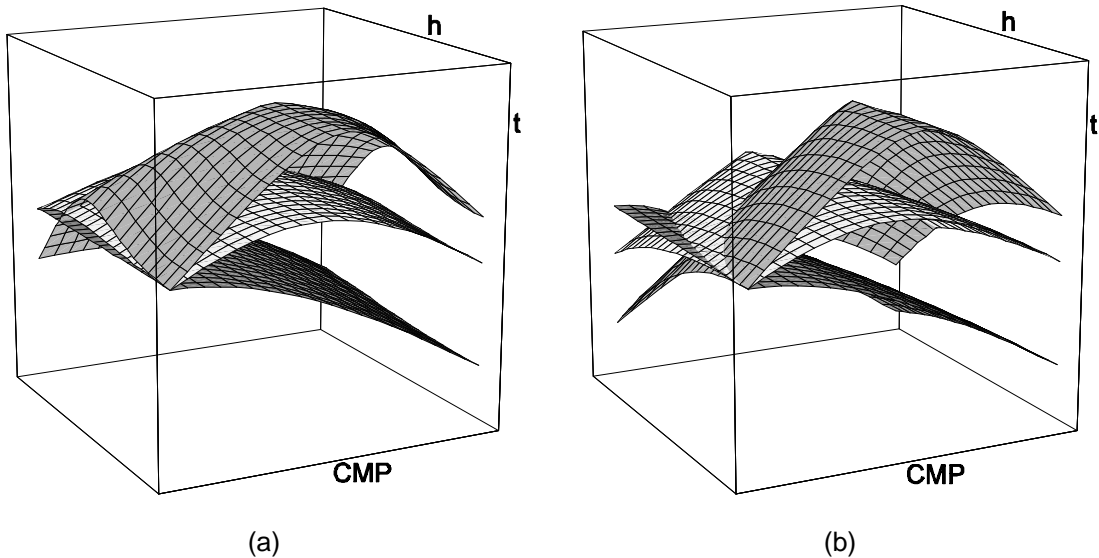


Fig. 7. Cheop's pyramids in an increasing velocity medium showing a) with NMO, and b) with NMO and DMO.

Constant offset and source (shot) record prestack migration

Data in constant offset sections, and source records, are convenient data organizations to apply NMO and DMO. The result of either process would create a figure similar to Figure 6 in which data from one scatter point will appear to be the same at all offsets. The addition of a zero offset (post stack) migration would collapse the cylindrical hyperbola to a line of energy at the scatter point. Stacking would complete the prestack migration process. (Note that an identical result would be produced by stacking first, followed by one zero offset migration). Once again this process only applies to constant velocity data where data from all scatter points would align on a CMP gather.

One reason for applying the migration to each constant offset section or source record before stacking is to attempt an improvement in velocity analysis. Typically inverse NMO (INMO) is applied, and the data processed with an additional round of velocity analysis. This process will allow an approximate velocity in a *constant* velocity field to converge to the correct velocity, and may be extended to areas with smoothly varying velocities. This process however, is flawed for structured data when INMO is applied at offsets that do not match the distance from the scatter point to the source and receiver (Bancroft 1995b).

DMO before NMO

Gardner's method of DMO before NMO (Forel and Gardner 1988) reconstructs the energy from Cheop's pyramid in Figure 2a to the hyperboloid in Figure 2b. The energy from other scatter points is also hyperbolic, but their shapes will lie on different paths due to the different velocities. Once again, the conventional NMO that follows will use some form of an average from the velocities of the surrounding scatter points.

Any NMO, DMO, or migration process that uses CMP gathers will be limited in its ability to produce an accurate image or to resolve velocities.

Prestack migration

All these above processes are attempting to collapse the energy of the Cheop's pyramid surface to the scatter point, and emulate full prestack Kirchhoff time migration in which the time T is computed from the DSR equation (2). The current limitation of these methods is the time and resulting costs required for processing.

The method presented in this paper achieves the same results as full Kirchhoff prestack time migration with the advantage of much shorter run times. In addition, an intermediate step forms gathers similar to PSI from which scatter point velocities may be estimated before NMO. The method is simple, easy to implement, and still uses most of the current processing algorithms such as velocity analysis.

Use of Kirchhoff migration requires care with the potential problem of aliasing, as recently described by Lumley (1993, 1994a and b). Aliasing occurs at the steeper dip

of the summing diffraction (or Cheop's pyramid). Its prevention requires the input trace to be high cut filtered at that sample and for the dip of the respective scatter point. Consequently, anti aliasing filters (AAF) are expensive to implement with full Kirchhoff prestack time migration.

PRESTACK MIGRATION GATHERS

In 1986, Stolt (page 36) expressed the desire for an operator "which migrates the unstacked data, but leaves NMO and stack undone". In a subsequent figure (1.17) Stolt illustrates an offset gather similar to a CMP gather, but which apparently contains all the input traces sorted by offset. In the same year, Gardner described a practical method based on DMO before NMO that formed a gather of energy from the input traces. More recently Ferber (1994) described an alternate method based on Gardners DMO.

This process may be described by reshaping the energy in the Cheop's pyramid to an hyperboloid, and then collapsing the three dimensional hyperboloid into a two dimensional hyperbola in the CMP plane. The offset in the CMP plane, for each input trace h_g is defined by

$$h_g^2 = h^2 + x_{mig}^2, \quad (6)$$

where h is the source/receiver offset, and x_{mig} is the distance from the CMP location to the migrated position of the scatter point. The hyperbolas are aligned for the appropriate CMP location, and for the correct velocity. Accurate velocity analysis may be performed on these gathers, which then require NMO, scaling, stacking, and filtering to complete the prestack migration. The method to be presented in this paper is similar to this approach in forming what we refer to as common scatter point (CSP) gathers.

A processing sequence with similar objectives creates a gather by first applying the DSR time shifting to the input trace, assigns an offset to the trace, applies inverse NMO for that offset, and then stacks this trace into the gather. The gather now contains all the prestack traces and is ready for further velocity analysis.

These methods create gathers with a very high fold and with offsets that can be much greater than the maximum source receiver offset. As a consequence, these gathers allow more accurate velocity analysis than is possible with conventional CMP gathers. (In typical 2-D data, a number of CMP's must be bunched to achieve a fold of one at each offset). Once the velocities have been evaluated, NMO and stacking completes the prestack migration.

The creation of the prestack migration gathers in this paper will be referred to as CSP gathers as they are based on the scatter point principles of Figure 1. The formation of these CSP gathers is not only much faster and simpler than the above methods, but it may also create CSP gathers at any arbitrary location within a 3-D

volume for velocity analysis, or may be used to quickly extract an arbitrarily located prestack migrated 2-D line from the 3-D volume.

The CSP gathers should not be confused with the CMP gathers formed after either shot record migration, or the migration of constant offset section. The CMP's are limited to the maximum offset of the source and receiver, and do not position the prestack energy in an optimum position for velocity analysis. Once NMO and even DMO has been applied, the data is essentially at zero offset and any arbitrarily assigned offset could be used for INMO. It is the contention of this paper that the offsets used for velocity analysis should be based on an offset that is related to the distances from the source and receivers to the CSP location, and not simply based on the source/receiver offset.

The CSP gathers are formed when samples in the input traces are assigned an offset that is based on the distance between the source/receiver positions relative to each CSP location. This offset is referred to as the *equivalent offset*. Once this offset is assigned, the input trace is then summed directly into the offset bins of the CSP gather. No time shifting of the input data is required. In the following sections, a simplified equivalent offset will be introduced that is based on NMO and post stack migration, and then followed with the complete definition based on prestack migration.

The new method presented in this paper is based on the full prestack Kirchhoff time migration, but runs much faster. The speed increase results when all the prestack traces for a given CSP are combined into offset bins before the kinematic computation. In addition, the DSR equation is replaced by conventional NMO. The actual number of floating point computations may be reduced on the order of 1000 for a 3-D resulting in overall speed improvements in the 100's. In addition, these CSP gathers allow scaling, filtering, and velocity analysis prior to any kinematic computations. These speed improvements are relative to the full prestack Kirchhoff method.

EQUIVALENT OFFSET DEFINITIONS

Equivalent offset from NMO and post-stack migration

In conventional NMO and post-stack migration, energy from each input trace is spread to all output traces similar to prestack migration. Energy is moved from the original two way time position T by NMO to the zero offset two way time T_{0-nmo} by

$$T^2 = T_{0-nmo}^2 + \frac{4h^2}{V_{rms}^2}, \quad (7)$$

where h is half the source/receiver offset. Energy may then be moved from the zero offset at two-way time T_{0-nmo} to the migrated two-way time at T_{0-mig} by the kinematic Kirchhoff migration equation

$$T_{0-nmo}^2 = T_{0-mig}^2 + \frac{4x_{off}^2}{V_{rms}^2}, \quad (8)$$

where x_{off} is the offset between the CMP and migrated position. These two equations may be combined to move energy directly from the input trace to the migrated position, by substituting (8) into (7) to give

$$T^2 = T_{0-mig}^2 + \frac{4(h^2 + x^2)}{V_{rms}^2} = T_{0-mig}^2 + \frac{4\tilde{h}_e^2}{V_{rms}^2}, \quad (9)$$

giving an initial estimate of the equivalent offset term \tilde{h}_e ,

$$\tilde{h}_e = h^2 + x_{off}^2. \quad (10)$$

A process may now be defined that combines NMO and post-stack migration into one step with the offset defined in equation (10) and a conventional NMO. This is now a prestack migration process utilizing Kirchhoff migration principles, requiring the use of offset scaling, antialiasing filters, and phase compensating filters. This process is schematically illustrated in Figure 8, which contains a prestack volume defined by half source/receiver offset, CMP trace position, and time. This figure relates to 2-D data with one axis defining the CMP location, however similar concepts apply for 3-D data. The shaded area in Figure 8 represents a CMP gather, and includes one example of an input trace at a CMP location and with offset h . The hyperbolic curves on the CMP gather represent the time shifting paths taken by data during NMO and stacking. The front surface of the volume represents a stacked or zero offset section. The zero offset section contains an arbitrarily located migrated trace with hyperbolas also showing the time shifting paths for migration. Note the data path taken by conventional NMO and post-stack migration as it first moves energy to the zero offset position and then to the migrated position. In contrast, the top surface shows the direct path of the combined process that uses the equivalent offset \tilde{h}_e to move energy from the input trace directly to the migrated position.

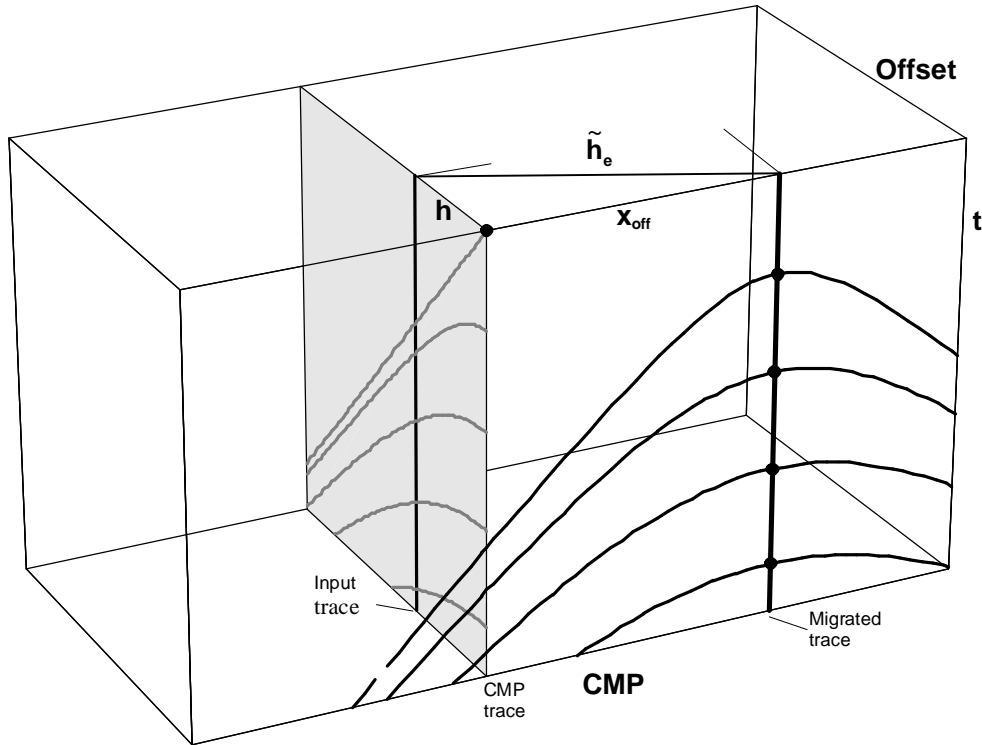


Figure 8. Prestack volume for 2-D data with dimension of offset, CMP position and time. Energy in an input trace on the CMP gather (shaded) will move to zero offset with NMO, and then to the migrated position.

The equivalent offset \tilde{h}_e allows all the input traces to be gathered prior to NMO, for a given migrated position as illustrated in Figure 3. This figure illustrates the same input trace in Figure 2 being copied into a bin of the CSP gather (shaded) at the offset defined by \tilde{h}_e . The NMO curves required for the prestack migration are also shown on the shaded migration gather. The intersection points of the grid on the top surface of Figure 9 is used to identify the position of other input traces positioned by CMP and offset h . All these traces may be assigned an equivalent offset and copied onto the prestack migration gather. These equivalent offsets may be much larger than the maximum source receiver offset which is illustrated by extending the shaded area of the gather beyond the maximum source receiver offset. When the migration position is moved, the input traces will be assigned different equivalent offsets.

The equivalent offset may also be evaluated with NMO compensated for dip by

$$T^2 = T_{0-nmo}^2 + \frac{4h^2 \cos^2(dip)}{V_{rms}^2} = T_{0-nmo}^2 + \frac{4h^2(1 - \sin^2(dip))}{V_{rms}^2}. \quad (11)$$

When combine with equation (8)

$$T^2 = T_{0-mig}^2 + \frac{4(h^2 + x^2 - h^2 \sin^2(dip))}{V_{rms}^2} = T_{0-mig}^2 + \frac{4\tilde{h}_e^2}{V_{rms}^2}, \quad (12)$$

giving another estimate of the equivalent offset term \tilde{h}_e ,

$$\tilde{h}_e = h^2 + x_{off}^2 - h^2 \sin^2(dip). \quad (13)$$

This form is not very useful as the dip must be predetermined, or many passes made with differing dips and dip filters.

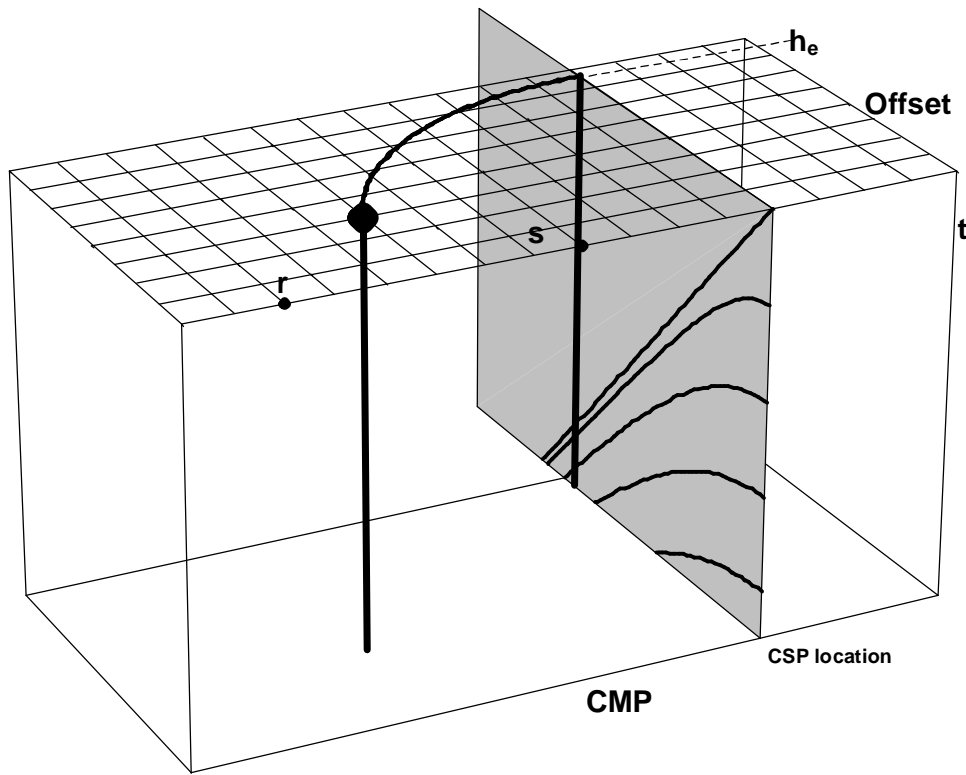


Fig 9. 2-D prestack volume illustrating movement of energy from the input trace to the prestack migration gather.

The equivalent offset from prestack migration

The above definition of the equivalent offset may be improved by incorporating the DSR equation into its definition. This is accomplished by defining a new source and receiver that are *collocated* at the equivalent offset position E in Figure 10. The equivalent offset is chosen to maintain the same total travel times as the original path (dashed) by the single two way path shown as the solid line.

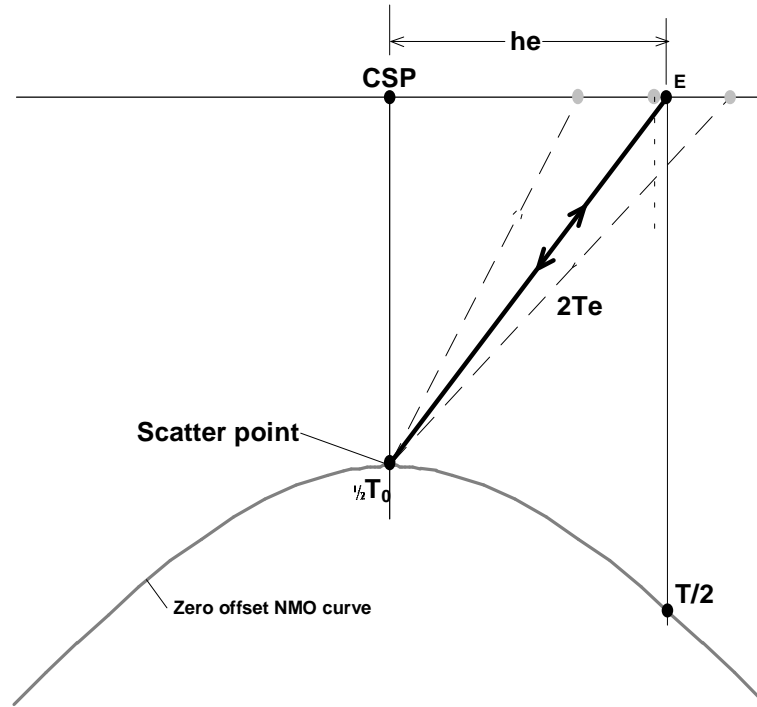


Fig. 10. Prestack migration illustration containing the equivalent offset position for a collocated source and receiver.

In forcing the source and receiver to be collocated, and positioned at the equivalent offset, the reflection time is now located on a hyperbola centered at the scatter point as illustrated in Figure 10. Once again NMO and stacking complete the prestack migration. Equation (1) is modified to include the equivalent offset one-way time T_e to become

$$2T_e = T_s + T_r = T \quad (15)$$

and when substituting the raypath parameters and using *one-way* times, we get

$$2 \left(\frac{1}{2} T_{0-mig}^2 + \frac{h_e^2}{V_{rms}^2} \right)^{1/2} = \left(\frac{1}{2} T_{0-mig}^2 + \frac{h_s^2}{V_{rms}^2} \right)^{1/2} + \left(\frac{1}{2} T_{0-mig}^2 + \frac{h_r^2}{V_{rms}^2} \right)^{1/2}. \quad (16)$$

The RMS velocities are all defined at the scatter point. Solving for h_e we obtain

$$h_e^2 = 0.25 \left[\left(\frac{1}{2} T_{0-mig}^2 V_{rms}^2 + h_s^2 \right)^{1/2} + \left(\frac{1}{2} T_{0-mig}^2 V_{rms}^2 + h_r^2 \right)^{1/2} \right]^2 - \frac{1}{2} T_{0-mig}^2 V_{rms}^2. \quad (17)$$

When the source and receiver are both on the same side of the CSP location (2-D data) as in Figure 1, then the half source/receiver offset h and the CMP to CSP distance x_{off} , are defined by

$$h = \frac{\left| |h_s| - |h_r| \right|}{2} \quad \text{and} \quad x_{off} = \frac{|h_s| + |h_r|}{2}, \quad (18), \text{ AND } (19)$$

or

$$h_s = x_{off} \pm h \quad \text{AND} \quad h_r = x_{off} \mp h. \quad (20), \text{ AND } (21)$$

Input 2-D traces in which the source and receiver straddle the CSP, and all input 3-D traces, may be converted into a geometry similar to Figure 1 by rotating the raypaths to be in a common vertical plane. Equations (18) and (19) will now be used as a general definition of h and x_{off} - *not* of the actual 3-D surface geometry. Azimuthal information of the source and receiver rays should still be preserved and used for azimuthal stacking.

Substituting equations (20) and (21) into equation (16), a more useful full definition of the equivalent offset is

$$h_e^2 = x_{off}^2 + h^2 - \left(\frac{2x_{off}h}{TV_{rms}} \right)^2. \quad (22)$$

The algebra is in the Appendix 2. Equation (22) may be used to map Cheop's pyramid energy in an input trace directly to the hyperboloid, or to copy energy into the CSP gather.

An equation that is similar to (16) may be derived by using square root approximations for the source and receiver raypath in equation (16), but the result contains the two-way zero offset time T_0 instead of the total two-way time T and is also derived in Appendix 3. When the square root approximation is used for all the terms in equation (16), the result is the same as equation (10) which was derived from NMO and post-stack migration. Its derivation appears in Appendix 4. The results of appendix 3 and 4 have been included for comparative purposes and to emphasize the desired result of equation (22).

The equivalent offset h_e defined in equation (22) is time or depth varying, and also a function of velocity. An input trace may have its sample spread over a number of offset bins, however the time samples still remain at the same time. An example of the time varying equivalent offset is shown in Figure 11 that shows the source and receiver positions s and r relative to the CSP location. Note the first useful energy in the input traces comes at a time T_α defined as the reflection from a scatter point at the surface of the CSP location and is given by

$$T_\alpha = \frac{2h_{cmp}}{V_{rms}}, \quad (23)$$

with an offset $h_{e\alpha}$ defined by

$$h_{e\alpha} = x_{off} \cdot \tag{24}$$

Energy at this point will migrate to the surface of the CSP trace with a dip of 90 degrees. The energy contribution to the CSP remains below T_α , where the offset increases slightly and tends to an offset asymptote $h_{e\omega}$ given by

$$h_{e\omega}^2 = x_{off}^2 + h^2, \tag{25}$$

which is also the same offset given by equation (7), derived from NMO and post-stack migration.

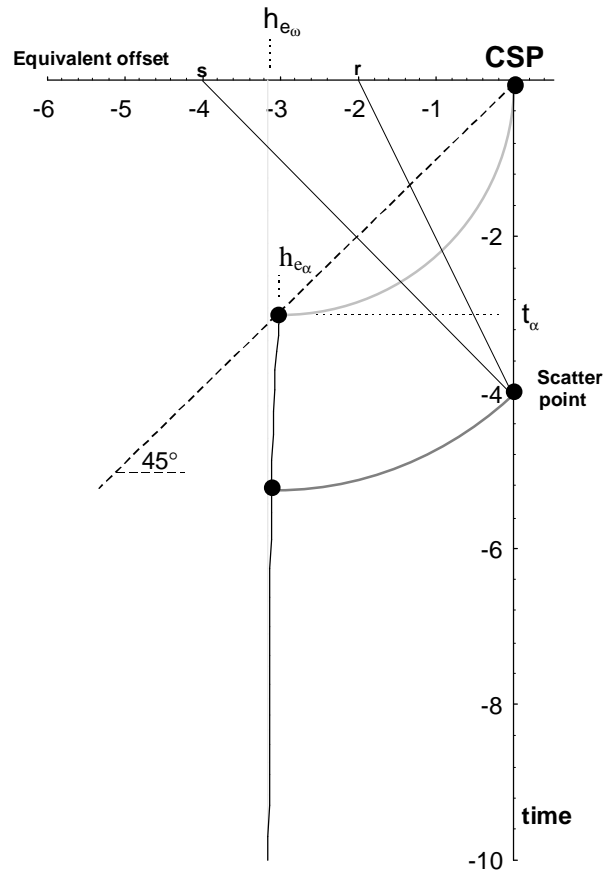


Fig. 11. Example of the time varying equivalent offset position.

FORMATION OF CSP GATHERS USING EQUIVALENT OFFSETS

It may appear from equation (22) that that the equivalent offset needs to be computed for each input sample. Fortunately that is not the case as only times at which the input samples start in a new bin need to be computed. The first useful sample on an input trace will come from a reflection off the scatter point at the surface. The travel time to this scatter point is T_α , and these positions lie at a 45 degrees angle on the CSP gather as illustrated in Figure 11. An initial equivalent offset

$h_{e\alpha}$ may be computed from this time and assigned to an appropriate offset bin with central offset $h(n)$ and incremental offset δh . The following samples are added to this bin until the equivalent offset increases to $h(n) + \frac{1}{2}\delta h$, at which point the samples are then added to the next offset bin $h(n+1)$. The time at which this occurs is $T(n+1)$ and may be found from rearranging equation (22) to give

$$T(n) = \frac{(2x_{\text{off}}h)}{V_{\text{rms}}(T_0)[x_{\text{off}}^2 + h^2 - h_e^2(n)]^{1/2}}. \quad (26)$$

In a similar manner, the transition times for all the offset bins may be computed, to allow efficient copying of the input trace samples into the respective bins.

The above assumption of using T_α as the starting time for an input trace assumes that the energy will propagate to time zero and correspond to a 90 degree migration. Time migrations to this steep angle may be impractical and include a great deal of unwanted noise. Limiting the extent of the migration angle is a popular feature of Kirchhoff migrations and it may also be applied to the formation of the CSP gathers. The pre-migration dip angles on the CSP gather may also be limited to reduce the noise, with an additional benefit of reducing the number of offset bins used by an input trace. In many cases, the number of offset bins may be reduced to one offset at h_{e0} . This benefit also occurs when half offset h is small relative to x_{off} , or when the first useful scatter points are below the surface as in marine data. The equivalent offset in equation (26) may also be used to define the time at which all remaining samples fall into the last bin.

In conventional Kirchhoff migrations, considerable effort is taken to postpone as much scaling and filtering as possible from the summation part of the process to save computing time (Silva 1992). This is not the case for CSP gathers as these operations may be applied efficiently before NMO and summation with little extra overhead. Application of the 3-D differential filter (root differential filter for 2-D) before NMO and summation also aids in focusing the velocity energy on semblance plots to aid in velocity analysis. In addition, other parameters such as dip range may also be applied to the CSP gathers and tested to optimize their effect on the final migration.

The size of the bin spacing δh in a CSP gather may be determined from the maximum allowable time shift which results from applying NMO to neighbouring bins. This value will depend on the frequency content of the data and the acquisition geometry. The effect of finite bin size with the high fold, and an assumed linear distribution, is to box car filter the binned data with period equal to the time shift. This filter has the same parameters as one required for antialiasing and in effect provides a natural filter for the data in a CSP gather. In practice, the bin spacing in the CSP gathers is less than that of the 3-D subsurface grid (or CMP spacing for 2-D) which require a more severe anti aliasing filter criteria. It is important to note that the bin size has little effect on the time required for acquiring the CSP gathers as the same number of input samples are summed. Smaller bin sizes require more offset bins, so

the memory requirements to save the offset will however increase. It should also be noted that the offset bin size should not be confused with the offset bin sizes in constant offset migration where the number of offset bins tend to be small to expedite the algorithm.

After the gathering, scaling, and filtering of the CSP gathers, the remaining processing steps to complete the prestack migration are NMO and stacking. Regular processing software may be used, along with conventional velocity analysis techniques. The only new software required is a routine to define the equivalent offset, and a routine to add the input energy to the appropriate offset bin.

PROPERTIES OF THE CSP GATHER

A comparison between the fold of the CMP gather and the prestack migration gather may be visualized from Figure 9. A CMP gather contains 9 traces from the grid, while the CSP gather could contain 153 traces. In real 2-D data, the CMP gather may contain only 15 live traces for a maximum possibility of 60 bins, while the corresponding CSP gather may contain tens of thousands of input traces spread over a few hundred bins. A CSP gather from 3-D data may contain hundreds of thousands of input traces. This extremely high fold and large offsets enable accurate velocity analysis at each migrated position. In contrast several CMP gathers may be required to obtain a single fold coverage for conventional velocity analysis.

An important property of the CSP gather is that many traces are summed using only the asymptotic equivalent offset $h_{e\omega}$. This data is independent of both time and velocity, providing stability to the CSP gather when the velocities are unknown. The CSP gathers may be formed with an arbitrary velocity, and the gather used to define a more accurate velocity. The iterations of this process converge very rapidly, and usually only one iteration is required. Velocities derived from the CSP gather are RMS type velocities.

The increased offset range of the CSP gather, and its high fold improve the resolution of velocity analysis. Consequently, the velocities on semblance plots focus to smaller points than on conventional semblance plots formed from a CMP gather. The better focusing of the data on semblance plots also illustrate the improved resolving power of prestack migration, and that the velocities must be quite accurate to enhance the signal and reduce the energy of multiples. This feature of the CSP gather may have substantial implications on field designs that are based on CMP gathers. In addition to the benefits of prestack migration, the standard algorithms for noise or multiple removal that were designed for use with CMP gathers may also be applied directly to CSP gathers.

This paper has used prestack migration to define CSP gathers based on equivalent offsets. Other criteria for forming the gathers may also be included. For example, azimuth restrictions may be applied to 2-D or 3-D data. Additional applications allow

the inclusion of converted wave velocity analysis and prestack migration. The method has also been used for crooked line processing

POSSIBLE ADDITIONAL BENEFITS OF THE CSP GATHERS

Static analysis is an area in which the CSP gather may also be of significant benefit. When conventional 2-D lines are recorded with source points at four-station intervals, four independent (de coupled) surface consistent solutions are obtained. Each receiver only contributes to every fourth CMP, requiring filtering techniques to combine the solutions. In addition the static solutions are obtained on NMO'ed data by correlating each input traces with a model that is typically a smoothed brute section. The CSP gather, in contrast to a CMP gather, contains many contributions from all sources and all receivers within the prestack migration aperture. This greatly increases the number of correlations and ensures the coupling of all sources and receivers with all CSP's. The high fold of the CSP gather may enable it to serve as a model for the input traces before NMO, to give statics that are independent of the stretching due to NMO. The success may possibly depend on removing coherent noise to create a suitable CSP gather model for correlating input traces.

Many traces in a CSP gather are positioned with offsets close to the asymptote $h_{e_{\omega}}$ and are therefore independent of time and velocity. When CSP gathers are produced independent of time and velocity, the potential applications may exceed those of prestack time migration. Time migrations with more complex moveout equations are possible and may be a necessity for taking advantage of the long offsets. In addition the accurate velocities derived from the CSP gathers may allow an accurate estimation of average velocities to produce an approximate depth migration.

CSP gathers may be formed to bias the azimuth of a ray path from either the source to scatter point, or the scatter point to receiver. Ray paths with a desired azimuth of one ray path leg may be collected with the azimuth of the other leg left to vary randomly within the high fold of the CSP gather. Comparison between biased azimuths may allow a better estimate of anisotropy velocities, and better prestack migrations. The processing time of biased azimuths will only double the stack time of CSP gather as each input trace will require summing into azimuth for each leg other total ray path.

CONVERTED WAVE PROCESSING

Converted wave processing assumes the downward propagating ray path is a P wave, and the reflection converts some P wave energy into shear wave that propagates to the surface. Recording of this shear wave with 3 component receivers provides additional information about the reflecting or converting surface, and allows the estimation of properties such as Poisson's ratio. The principle of equivalent offsets may also be applied to this processing scheme to provide a better velocity analysis, simplify and speed the processing, and give improved results. The processing method start with the DSR equation with the appropriate P and S velocities for each leg of the

ray path. The equivalent offset will enable the formation of a common conversion scatter point (CCSP) gather with hyperbolic data suitable for conventional velocity analysis and processing. The processing is more complex than the conventional P-P wave processing, and the details are contained in a companion paper by Wang (Chapter 27).

CONCLUSIONS

A robust method of prestack migration has been developed that is simpler and much faster than conventional methods. It is based on Kirchhoff prestack time migration, but modifies the migration process to gathering, NMO, and stacking. The new method correctly maps energy from prestack traces to equivalent offsets in common scatter point (CSP) gathers. Conventional velocity analysis tools may be used on the CSP gathers to accurately determine RMS velocities. Other advantages may include coupled surface consistent statics, improved field design, converted wave processing, multiple evaluation and simplified processing.

ACKNOWLEDGMENTS

We wish to thank the sponsors of the CREWES Project for their support. The technical support from Henry Bland was greatly appreciated.

REFERENCES

- Bancroft, J. C., and Geiger, H. D., 1994 equivalent offsets and CRP gathers for prestack migration, Expanded Abstracts 1994 SEG International Convention, pp. 672-675.
- Bancroft, J. C., Geiger, H. D., Foltinek, D. S., and Wang, S., 1994 Prestack migration by equivalent offsets and CSP gathers, CREWES 1994 Research Report.
- Bancroft, J. C., and Wang, S., 1994, Converted-wave prestack migration and velocity analysis by equivalent offsets and CSP gathers, CREWES 1994 Research Report.
- Bancroft, J. C., Wang, S., Foltinek, D. S., and Geiger, H. D., 1995 Common scatter point (CSP) prestack migration, 1995, Expanded Abstracts CSEG 1995 National Convention.
- Bancroft, J. C., 1995b, Velocity sensitivity for equivalent offset in CSP gathers, CREWES 1995 Research Report.
- Claerbout, J. F., 1985, *Imaging the Earth's Interior*, Blackwell Scientific, (out of print) available through Email
- Deregowski, S., 1986, What is DMO?, *First Break*, Vol. 4, pp. 7-24
- Deregowski, S. M., 1990, Common-offset migrations and velocity analysis, *First Break*, Vol. 8, 225-234
- Denelle, E., Dezard, Y., and Raoult, J. J., 1986, 2-D prestack depth migration in the (S-G-W) domain, *Exp. Abs., SEG Nat. Convention.*, pp. 327-330
- Diet, J. P., Audebert, F., Huard, I., Lanfranchi, P., and Zhang, X., 1993, Velocity analysis with prestack time migration using the S-G method: A unified approach, Technical Program, SEG National Convention. 63rd Ann. Int. Mtg., Washington, D. C., pp. 957
- Dix, C. H., 1955, Seismic velocities from surface, *Geophysics*, Vol. 20, pp. 86-86
- Ferber, R. G., 1994, Migration to multiple offset and velocity analysis, *Geophy. Prosp.*, Vol. 42, pp. 99-112
- Forel D., and Gardner, G., 1988, A Three-Dimensional Perspective on Two-Dimensional Dip Moveout, *Geophysics*, Vol. 53, pp. 604-610

- Gardner, L. W., 1947, Vertical velocities from reflection shooting, *Geophysics*, Vol. 12, pp. 221-228
- Gardner, G. H. F., Wang, S. Y., Pan, N. D., and Zhang, Z., Dip moveout and prestack imaging:, 1986, *Offshore Technology Conference*.
- Geiger, H., Bancroft, J. C. and Foltinek, D., 1995, Prestack migration of crustal data using common scatter point (CSP) migration technique, *Expanded Abstracts CSEG 1995 National Convention*
- Lee, W. B. and Zhang, L., 1992, Residual shot profile migration, *Geophysics*, Vol. 57, pp. 815-
- Lindsey, J. P., and Herman, A., 1970, Digital migration, *Oil and Gas Journal*, 38, 112-115, (also in *Migration of Seismic Data*, SEG reprint series)
- Lumley, D. E., 1989, A generalized Kirchhoff-WKBJ depth migration theory for multi-offset seismic reflection data: reflectivity model construction by wavefield imaging and amplitude estimation., *Masters Thesis, University of British Columbia*
- Lumley, D. E., and Claerbout, J. F. 1993, Anti-aliased Kirchhoff 3-D migration: a salt intrusion example, *SEG 3-D Seismic Workshop*, pp. 115-123
- Lumley, D. E., Claerbout, J. F., and Bevc, D., 1994, Anti-aliased Kirchhoff 3-D migration, *Exp. Abs. SEG National Convention*, pp. 1282-1285
- Lumley, D. E., Claerbout, J. F., and Bevc, D., 1994, Anti-aliased Kirchhoff migration, *Exp. Abs. EAEG Technical Exhibition*, pp. H027
- Ng, M., 1993, *Prestack migration of shot records*
- Rockwell, D. W., 1971, Migration stack aids interpretation, *Oil and Gas Journal*, 69, 202-218, (also in *Migration of Seismic Data*, SEG reprint series)
- Sattlegger, J. W., Stiller, P. K., Echterhoff, J. A., and Hentschke, M. K., 1980, Common offset plane migration (COPMIG), *Geophys. Prosp.*, Vol. 28, pp. 859-871
- Schultz, P. and Sherwood, 1980, Depth migration before stack, *geophysics*, Vol. ,pp. 376-393
- Silva, R., 1992, Antialiasing and application of weighting factors in Kirchhoff migration, *Technical Program, Soc. Expl. Geophys. 62nd Ann. Int. Mtg.*, New Orleans, pp. 995-998
- Stolt, R. H., and Benson, A. K., *Seismic Migration, Theory and Practice*., 1986, *Geophysical Press*. (See page 36)
- van der Schoot, A., Romijn, R., Larson, D. E., and Berkhout, A. J., 1989, Prestack migration by shot record inversion and common depth point stacking: a case study, *First Break*, Vol. ,pp. 293-304
- Wang, S., Bancroft, J. C., Foltinek, D., and Lawton, D., 1995, Converted -wave (P-SV) prestack migration and velocity analysis, *Expanded Abstracts CSEG 1995 National Convention*
- Westbroek, H., and Stewart, R., 1995, Imaging rugose targets using 2-D and 3-D migration, *Expanded Abstracts CSEG 1995 National Convention*

APPENDIX 1. DERIVATION OF STACKING VELOCITY FROM THE DSR EQUATION

The curvature of the Cheop's pyramid at a position x (defined as the distance from the scatter point to CMP position) may be found from the DSR equation (2) using the half source/receiver offset h . The zero offset time at the scatter point is defined as T_{0-mig} , and the zero offset time at the CMP is defined as T_{0-nmo} . For simplicity, the velocity at the scatter point $V(T_{0-mig})$ is simplified to V , to give

$$T = \sqrt{\frac{1}{2}T_{0-mig}^2 + \frac{(x+h)^2}{V^2}} + \sqrt{\frac{1}{2}T_{0-mig}^2 + \frac{(x-h)^2}{V^2}}. \quad (A1)$$

The curvature is evaluated from the second derivative, evaluated at the CMP position x , and as h tends to zero to giving

$$\left. \frac{d^2T}{dh^2} \right|_{h \rightarrow 0} = \frac{4T_{0-mig}^2}{V^2 T_{0-nmo}^3}. \quad (A2)$$

The times are now two-way times to compare with a hyperbolic NMO curve

$$T^2 = T_{0-nmo}^2 + \frac{4h^2}{V_{stk}^2}, \quad (A3)$$

where the velocity V_{stk} is chosen to give "the best stack." The second derivative of this hyperbola as h tends to zero is

$$\left. \frac{d^2T}{dh^2} \right|_{h \rightarrow 0} = \frac{4}{T_{0-nmo} V_{stk}^2}. \quad (A4)$$

Equating equations (A2) and (A4) give the NMO velocity

$$V_{stk} = V \frac{T_{0-nmo}}{T_{0-mig}} = \frac{V}{\cos(dip)} \quad (A5)$$

which is the familiar velocity correction required for stacking a dipping event located at the scatter point. Note the velocity V is the velocity at the scatter point T_{0-mig} and not at the NMO time T_{0-nmo} . Only the energy close to zero offset will be stacked using this method of processing.

**APPENDIX 2. DERIVATION OF THE EQUIVALENT OFFSET EQUATION
(16)**

The DSR equation (16) is modified by resorting and moving the velocity to get

$$\left[\left(\frac{1}{2} T_0 V \right)^2 + (x_{off} + h)^2 \right]^{1/2} = 2 \left[\left(\frac{1}{2} T_0 V \right)^2 + h_e^2 \right]^{1/2} - \left[\left(\frac{1}{2} T_0 V \right)^2 + (x_{off} - h)^2 \right]^{1/2} \quad (\text{A2-1})$$

then by squaring,

$$\begin{aligned} \left(\frac{1}{2} T_0 V \right)^2 + (x_{off} + h)^2 = & 4 \left[\left(\frac{1}{2} T_0 V \right)^2 + h_e^2 \right] + \left[\left(\frac{1}{2} T_0 V \right)^2 + (x_{off} - h)^2 \right] - \\ & 4 \left\{ \left[\left(\frac{1}{2} T_0 V \right)^2 + h_e^2 \right] \left[\left(\frac{1}{2} T_0 V \right)^2 + (x_{off} - h)^2 \right] \right\}^{1/2} \end{aligned} \quad (\text{A2-2})$$

expanding terms

$$\begin{aligned} \left(\frac{1}{2} T_0 V \right)^2 + x_{off}^2 + h^2 + 2x_{off}h = & 4 \left[\left(\frac{1}{2} T_0 V \right)^2 + h_e^2 \right] + \left(\frac{1}{2} T_0 V \right)^2 + x_{off}^2 + h^2 - 2x_{off}h - \\ & 4 \left\{ \left[\left(\frac{1}{2} T_0 V \right)^2 + h_e^2 \right] \left[\left(\frac{1}{2} T_0 V \right)^2 + (x_{off} - h)^2 \right] \right\}^{1/2} \end{aligned} \quad (\text{A2-3})$$

to get

$$\begin{aligned} 4x_{off}h = & 4 \left[\left(\frac{1}{2} T_0 V \right)^2 + h_e^2 \right] - \\ & 4 \left\{ \left[\left(\frac{1}{2} T_0 V \right)^2 + h_e^2 \right] \left[\left(\frac{1}{2} T_0 V \right)^2 + (x_{off} - h)^2 \right] \right\}^{1/2} \end{aligned} \quad (\text{A2-4})$$

resorting,

$$\left[\left(\frac{1}{2} T_0 V \right)^2 + (x_{off} - h)^2 \right]^{1/2} = \frac{4 \left[\left(\frac{1}{2} T_0 V \right)^2 + h_e^2 \right] - 4x_{off}h}{4 \left[\left(\frac{1}{2} T_0 V \right)^2 + h_e^2 \right]^{1/2}} \quad (\text{A2-5})$$

simplifying

$$\left[\left(\frac{1}{2} T_0 V \right)^2 + (x_{off} - h)^2 \right]^{1/2} = \left[\left(\frac{1}{2} T_0 V \right)^2 + h_e^2 \right]^{1/2} - \frac{x_{off}h}{\left[\left(\frac{1}{2} T_0 V \right)^2 + h_e^2 \right]^{1/2}} \quad (\text{A2-6})$$

squaring

$$\left(\frac{1}{2}T_0V\right)^2 + x_{off}^2 + h^2 - 2x_{off}h = \left(\frac{1}{2}T_0V\right)^2 + h_e^2 + \frac{(x_{off}h)^2}{\left[\left(\frac{1}{2}T_0V\right)^2 + h_e^2\right]} - 2x_{off}h \quad (\text{A2-7})$$

eliminating terms, and resorting

$$h_e^2 = x_{off}^2 + h^2 - \frac{(x_{off}h)^2}{\left[\left(\frac{1}{2}T_0V\right)^2 + h_e^2\right]} \quad (\text{A2-8})$$

and finally, the denominator term is simplified with the total two way time T to get the desired result.

$$h_e^2 = x_{off}^2 + h^2 - \left(\frac{2x_{off}h}{TV_{rms}(T_0)}\right)^2 \quad (\text{A2-9})$$

APPENDIX 3. APPROXIMATE DERIVATION OF THE EQUIVALENT OFFSET EQUATION

Starting with the DSR equation again,

$$2 \left[\frac{1}{2} T_0^2 + \frac{h_e^2}{V^2} \right]^{1/2} = \left[\frac{1}{2} T_0^2 + \frac{h_s^2}{V^2} \right]^{1/2} + \left[\frac{1}{2} T_0^2 + \frac{h_r^2}{V^2} \right]^{1/2} \quad (\text{A3-1})$$

and dividing by T_0

$$2 \left[1 + \left(\frac{h_e}{\frac{1}{2} T_0 V} \right)^2 \right]^{1/2} = \left[1 + \left(\frac{h_s}{\frac{1}{2} T_0 V} \right)^2 \right]^{1/2} + \left[1 + \left(\frac{h_r}{\frac{1}{2} T_0 V} \right)^2 \right]^{1/2}. \quad (\text{A3-2})$$

Recalling the expansion

$$(1+x)^{1/2} \approx 1 + \frac{x}{2} - \frac{x^2}{8} + \frac{x^3}{16} - \dots \quad (\text{A3-3})$$

substitute the series terms into (A3-2)

$$2 \left[1 + \left(\frac{h_e}{\frac{1}{2} T_0 V} \right)^2 \right]^{1/2} = \left[1 + \frac{1}{2} \left(\frac{h_s}{\frac{1}{2} T_0 V} \right)^2 - \frac{1}{8} \left(\frac{h_s}{\frac{1}{2} T_0 V} \right)^4 + \dots \right] + \left[1 + \frac{1}{2} \left(\frac{h_r}{\frac{1}{2} T_0 V} \right)^2 - \frac{1}{8} \left(\frac{h_r}{\frac{1}{2} T_0 V} \right)^4 + \dots \right] \quad (\text{A3-4})$$

which becomes

$$2 \left[1 + \left(\frac{h_e}{\frac{1}{2} T_0 V} \right)^2 \right]^{1/2} = 2 + \frac{1}{2} \frac{h_s^2 + h_r^2}{\left(\frac{1}{2} T_0 V \right)^2} - \frac{1}{8} \frac{h_s^4 + h_r^4}{\left(\frac{1}{2} T_0 V \right)^4} + \dots \quad (\text{A3-5})$$

Squaring both sides,

$$4 \left[1 + \left(\frac{h_e}{\frac{1}{2} T_0 V} \right)^2 \right]^2 = 4 + 2 \frac{h_s^2 + h_r^2}{\left(\frac{1}{2} T_0 V \right)^2} + \frac{\frac{1}{4} (h_s^2 + h_r^2)^2 - \frac{1}{2} (h_s^4 + h_r^4)}{\left(\frac{1}{2} T_0 V \right)^4} + \dots \quad (\text{A3-6})$$

and simplifying,

$$h_e^2 = \frac{1}{2} (h_s^2 + h_r^2) + \frac{(h_s^2 + h_r^2)^2 - 2(h_s^4 + h_r^4)}{16 \left(\frac{1}{2} T_0 V \right)^2} + \dots \quad (\text{A3-7})$$

or,

$$h_e^2 = \frac{1}{2}(h_s^2 + h_r^2) + \frac{h_s^4 + 2h_s^2 h_r^2 + h_r^4 - 2(h_s^4 + h_r^4)}{16\left(\frac{1}{2}T_0 V\right)^2} + \dots \quad (\text{A3-8})$$

Simplifying further,

$$h_e^2 = \frac{1}{2}(h_s^2 + h_r^2) - \frac{h_s^4 - 2h_s^2 h_r^2 + h_r^4}{16\left(\frac{1}{2}T_0 V\right)^2} + \dots \quad (\text{A3-9})$$

and further,

$$h_e^2 = \frac{1}{2}(h_s^2 + h_r^2) - \frac{(h_s^2 - h_r^2)^2}{16\left(\frac{1}{2}T_0 V\right)^2} + \dots \quad (\text{A3-10})$$

Recall

$$h_s = x_{off} + h \quad \text{and} \quad h_r = x_{off} - h. \quad (14), \text{ AND } (15)$$

then

$$h_s^2 + h_r^2 = 2(x_{off}^2 + h^2) \quad (\text{A3-11})$$

and

$$h_s^2 - h_r^2 = 4x_{off}h \quad (\text{A2-})$$

giving

$$h_e^2 = x_{off}^2 + h^2 - \frac{x_{off}^2 h^2}{\left(\frac{1}{2}T_0 V\right)^2} + \dots \quad (\text{A3-12})$$

and finally

$$h_e^2 = x_{off}^2 + h^2 - \left(\frac{2x_{off}h}{T_0 V}\right)^2 + \dots \quad (\text{A3-13})$$

Note in this approximation, time is T_0 not T .

APPENDIX 4. 2ND APPROXIMATE DERIVATION OF THE EQUIVALENT OFFSET EQUATION

Starting with equations (A3-2) and (A3-3)

$$2 \left[1 + \frac{1}{2} \left(\frac{h_e}{\frac{1}{2} T_0 V} \right)^2 - \frac{1}{8} \left(\frac{h_e}{\frac{1}{2} T_0 V} \right)^4 + \dots \right] =$$

$$\left[1 + \frac{1}{2} \left(\frac{h_s}{\frac{1}{2} T_0 V} \right)^2 - \frac{1}{8} \left(\frac{h_s}{\frac{1}{2} T_0 V} \right)^4 + \dots \right] +$$

$$\left[1 + \frac{1}{2} \left(\frac{h_r}{\frac{1}{2} T_0 V} \right)^2 - \frac{1}{8} \left(\frac{h_r}{\frac{1}{2} T_0 V} \right)^4 + \dots \right] \quad (A4-1)$$

Simplifying,

$$\left(\frac{h_e}{\frac{1}{2} T_0 V} \right)^2 - \frac{1}{4} \left(\frac{h_e}{\frac{1}{2} T_0 V} \right)^4 + \dots = \frac{1}{2} \frac{h_s^2 + h_r^2}{\left(\frac{1}{2} T_0 V \right)^2} - \frac{1}{8} \frac{h_s^4 + h_r^4}{\left(\frac{1}{2} T_0 V \right)^4} + \dots \quad (A4-2)$$

using only the second order terms

$$\left(\frac{h_e}{\frac{1}{2} T_0 V} \right)^2 - + \dots = \frac{1}{2} \frac{h_s^2 + h_r^2}{\left(\frac{1}{2} T_0 V \right)^2} - + \dots \quad (A4-3)$$

giving,

$$h_e^2 = \frac{1}{2} (h_s^2 + h_r^2) - + \dots \quad (A4-5)$$

but recall

$$h_s = x_{off} + h \quad \text{AND} \quad h_r = x_{off} - h. \quad (14), \text{ AND } (15)$$

and

$$h_s^2 + h_r^2 = 2(x_{off}^2 + h^2) \quad (A4-6)$$

giving

$$h_e^2 = x_{off}^2 + h^2 \quad (A4-8)$$